**Monitoring water content in deforming intervertebral disc tissue by finite element analysis of MRI data**

Kingma, I; van Dieën, J H; Nicolay, K; Maat, J.; Weinans, H.

# Monitoring Water Content in Deforming Intervertebral Disc Tissue by Finite Element Analysis of MRI Data

Idsart Kingma,[1*] Jaap H. van Dieën,[1] Klaas Nicolay,[2] Johan J. Maat,[1] and Harrie Weinans[3]

**Mechanical loading, occurring during normal daily life, causes fluid to be expelled from intervertebral discs. Excessive fluid loss during heavy loading might make the disc more vulnerable to damage. In this study, fluid loss was investigated in vitro through monitoring the loss of MRI signal intensity in four bovine coccygeal intervertebral discs, compressed at 2000 N during 1.5 hr. The MRI signals were analyzed with the aid of finite element models to account for the deformation of the tissue. A gradual signal loss over time was found during loading, the most pronounced loss occurring in the central disc region. Initial patterns of signal distribution were quite variable between specimens but repeatable within specimens. Magn Reson Med 44:650–654, 2000. © 2000 Wiley-Liss, Inc.**

**Key words: intervertebral disc; MRI; water content; finite element; tissue deformation**

Tissue motion is one of the major challenges in the application of MRI. For certain applications, the motion itself is the topic of interest (1), but for others, where the characteristics of the tissue are to be studied, tissue motion confounds the measurement. In some applications the imaging time as well as the time scale of tissue deformation is several orders of magnitude larger than the time allowed for correction by tagging and navigator techniques (2,3). An example is the measurement of fluid redistribution in a deforming intervertebral disc. Due to the absence of vascularization, fluid flow has a metabolic function in the disc (4). In addition, fluid loss due to compressive forces causes a redistribution of stress over the disc, resulting in stress peaks in the anulus (5), thereby enhancing the risk of damage, either to the vertebral endplate or to the anulus.

In a preliminary in vitro study, using one specimen and a linear elastic finite element model (6), it was suggested that finite element aided compensation for tissue deformation might be a feasible way to obtain a detailed map of signal intensity changes after a period of loading of intervertebral discs (7).

The aim of the current study was to refine and expand this method so that the time-dependent behavior of water content changes in loaded intervertebral disc tissue could be taken into account. For this purpose, serial MRI measurements were made during loading of bovine coccygeal intervertebral discs in vitro. The gradual deformation of the intervertebral disc tissue was followed with biphasic finite element models of the specimens. In these models, elastic properties of the solid part of the tissue are combined with flow properties of the fluid part of the tissue so that the time-dependent deformation due to fluid flow in the tissue can be simulated (8).

The reliability of the measurements was investigated by repeating them after about 20 hr.

## METHODS

### Specimen Dissection and Loading Protocol

Four coccygeal Functional Spinal Units (FSU's, one intervertebral disc plus two adjacent vertebrae) were dissected from four bovine tails. After embedding the top and bottom in Polymethyl-Methacrylate, the FSU's were stored in plastic bags at –20°C. Before the experiment, the FSU's were left to thaw while submersed in a normal saline solution at room temperature under an axial pre-load with a compressive force of 250 N. This load is comparable to the force on human discs in supine posture (9). After pre-loading for at least 15 hr, the FSU's were loaded at 2000 N during 1.5 hr within the receiver coil of the MR instrument, using a plastic loading device (Fig. 1). To prevent fluid loss through evaporation in the MR instrument, the FSU's had been wrapped in cling film. After recovery in saline at 250 N compression during about 20 hr, the loading procedure in the MRI coil was repeated.

### MRI Measurement

MRI measurements were made on a 4.7 Tesla MRI scanner (Varian / SISCO, Palo Alto, CA), equipped with a 33 cm diameter actively shielded gradient (max. gradient strength 32 mT/m). An 11 cm diameter Alderman–Grant type radio-frequency coil was used for signal excitation and reception. Each measurement, taking 12.48 min, consisted of an average of two shots of 31 transversal slices (0.5 mm thick) with a resolution of 0.9375 mm in the transversal plane (field of view 60×60 mm$^2$, TR/ TE = 6000/16 msec). Within the 1.5 hr loading period, seven MRI measurements were made for three out of four specimens. In one specimen (FSU 3) only five subsequent measurements were made as a consequence of a technical failure of the MRI system. A water-filled syringe, connected to a thin plastic tube (Fig. 1), was used to measure the axial displacement of the top vertebra (Fig. 2).

### Finite Element Aided Compensation for Tissue Deformation

A 2-dimensional (2D) circular mesh of finite elements was generated semi-automatically over each transversal MR
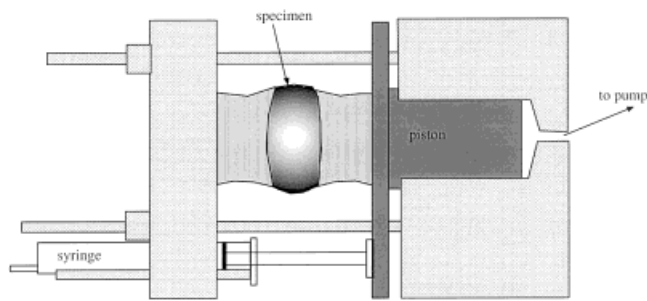
FIG. 1. The plastic loading device that was used to compress the FSU's within the MRI coil.

image (Fig. 3, top row). To avoid artifacts in the processing of MRI signals through the cling film or through a water film between the cling film and the tissue, a small margin was left between the outermost tissue margin and the outer contour of the model. Then the 2D element grids of the 31 transversal images were connected such that a 3D grid of elements was obtained, covering the disc and a part of both adjacent vertebrae. To obtain element regions that followed the contours of the vertebral endplate, parabolic deformations were applied in axial direction (Fig. 3, bottom row). In order to obtain realistic time-dependent tissue deformation, including diffusion and fluid loss, each element in the model was considered as consisting of fluid and solid at the same time. Material parameters for this so-called biphasic model were obtained from Argoubi et al. (10) and slightly adapted to obtain a good fit with the deformation behavior of the current specimens (Table 1).

For each of the four specimens, its measured axial compression was used to simulate the tissue deformation in the associated finite element model, using a commercially available finite element code (Diana, TNO Delft, The Netherlands). This code uses the constitutive equations of the classical theory of linear isotropic poroelasticity (11) as governing differential equations. Using this theory, stresses that are calculated at each nodal point in the model are assumed to be made up by a pressure stress carried by the fluid and an effective stress carried by the solid. The solid and fluid are assumed to be intrinsically incompressible and the creep behavior of the tissue is assumed to be purely poroelastic, with the fluid flow (q) relative to the solid being dependent on the permeability (k) and the fluid pressure gradient ($\nabla\phi$) according to Darcy's law:

$$q = -k\nabla\phi.$$

According to the assumption of purely poroelastic creep, the viscosity of the solid is set to zero.

The deformed model, at the time instant half way each MRI measurement, was saved for further analysis. In this way, each MRI measurement was coupled to one deformed model that simulated the instantaneous tissue deformation. Thus, assuming perfect simulation of tissue deformation, one element always represented exactly the same tissue fraction within each FSU. Next, the MR images were 'read' into the associated finite element model and the average signal intensity was calculated for each element (7). For the retest measurements on the second day, the whole procedure was repeated, including the development of new specimen-specific finite element models.

## RESULTS

The total axial deformation of the discs within the 1.5 hr loading (excluding the instant of load application) was between 0.5 and 1.0 mm during the first measurement and 0.3 to 0.5 mm during the retest (Fig. 2). The rate of deformation gradually decreased over time but did not reach zero within 1.5 hr. The time instants half way the MRI measurements (and consequently the deformations applied to the finite element models, associated with the specimens) are indicated by symbols.

To describe the signal intensities in functional regions, several element layers of the disc (see Fig. 3, bottom right) were averaged to obtain a caudal, medium, and cranial region. In addition, average values within the five central to peripheral element rings (see Fig. 3, top right) were calculated, separated for the three regions as well as averaged over regions. All averaged values were calculated after weighing for the volume of individual elements. The time series of signal intensities in the five central to peripheral disc rings (Fig. 4c and d), show a consistent decrease of signal intensity during compression of the disc. However, the outermost ring only shows marginal changes in all four specimens. Over all specimens, the signal decrease from the first to the last time step was 27.7±1.6, 29.6±11.6, 24.9±10.3, 10.2±5.2, and 2.0±1.7 units, from the innermost to the outermost ring. The strongest loss of signal intensity was found in the most central rings in specimens 3 and 4 and in the second most central rings in specimens 1 and 2. These differences can not simply be

FIG. 2. Curves of axial deformation of the specimens during loading on day 1 (left) and day 2 (right). The curves are exponential fits through the measured displacement of each top vertebra (R > 0.989 for all specimens). The symbols (star, circle, square, and triangle for specimen 1 to 4, respectively) indicate the time instant half way each MRI measurement. The axial deformation, read from the curves at these time instants, was applied to each specimen-specific finite element model.
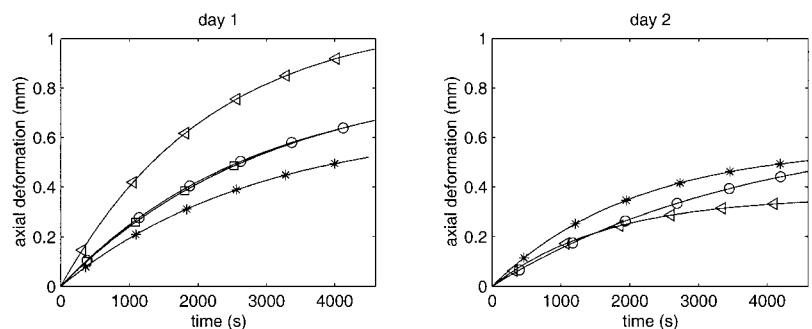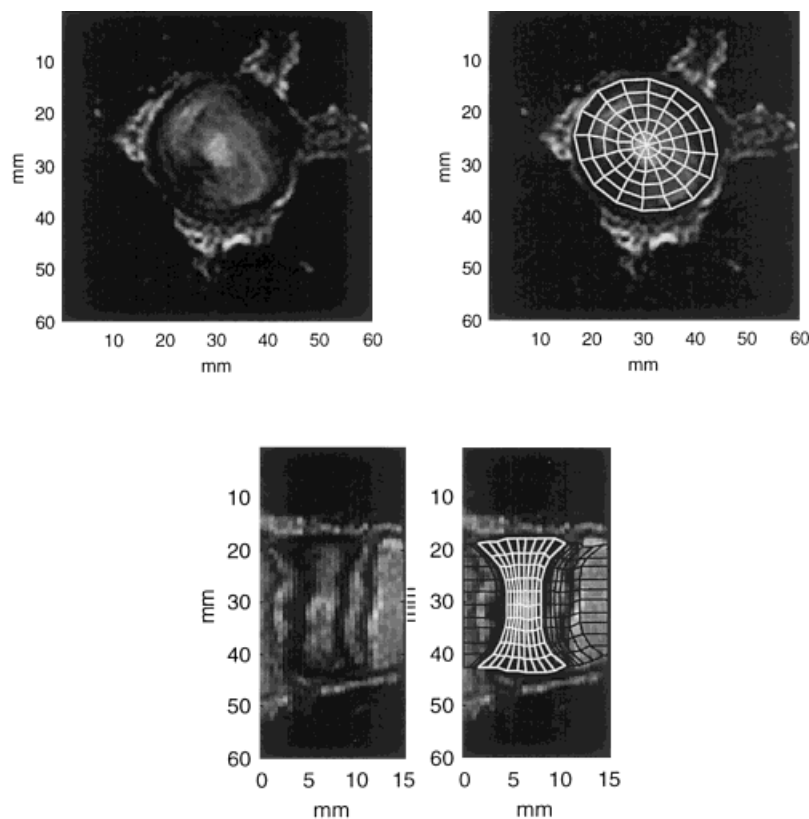
FIG. 3. Top: transversal MRI image through a bovine coccygeal intervertebral disc (specimen 2), just after the loading of the disc with 2000 N started. The right side shows the same image, with the circular finite element mesh that was generated over the image. Bottom: a sagittal reconstruction of the transversal images (2.3 mm thick). Such reconstructions were used to impose the curved shape of the vertebral endplates to the finite element models (right image). Note that in the bottom figures the scaling differs between the horizontal and vertical axes.

traced back to variations in initial signal content. Specimen 1, for example, showed the highest signal loss in ring 2 (just like specimen 2, Fig. 4c), but the initial signal content was relatively low in this ring (just like in specimen 4, Fig. 4b).

The signal distributions over rings (and their change over time) were similar in the caudal, central, and top region within each specimen. However, there were profound differences between specimens in signal distributions over rings (Fig. 4a and b). The retest measurements on the second day show a similar distinct pattern of signal distribution over rings within specimens (Fig. 5). Except for the most central ring in specimen 1, the signal content at the start of the loading period was considerably lower on the second day than on the first day (Fig. 5). This indicates that marginal recovery (water uptake) had oc-

curred between the last measurement of the first day and the first measurement of the second day, despite the fact that the specimens were fully submerged in saline throughout the recovery period.

## DISCUSSION

The biphasic finite element model appeared to be a useful method to track the time-dependent deformation of the intervertebral disc tissue in the current study. The experimental setup guaranteed correct overall vertical deformation. At a local level though, model assumptions, like pure poroelastic behavior and the use of isotropic material properties, may have resulted in small errors in the estimation of tissue deformation. However this is unlikely to have large influence on the current result since data were

Table 1
Material Parameter Values for the Finite Element Models

| Material | Young modulus (Mpa) | Poisson ratio | Permeability (mm$^4$ N$^{-1}$ s$^{-1}$) | Porosity |
|---|---|---|---|---|
| Trabecular bone | 100.0 | 0.2 | 0.0001 | 0.2857 |
| Cortical bone | 10000.0 | 0.3 | 1.0e-8 | 0.0196 |
| Endplates | 500.0 | 0.1 | 0.0001 | 0.8 |
| Anulus fibrosus | 20.0 | 0.1 | 0.00005 | 0.69997 |
| Nucleus pulposus | 5.0 | 0.1 | 0.00005 | 0.8 |

FIG. 4. Example of signal distribution (**a** and **b**) and signal intensity change (**c** and **d**) in two specimens during loading with 2000 N at the first day of measurements. In **a** and **b**, the horizontal axis represents the central to peripheral element rings. The numbered lines indicate the first (1) to last (7) MRI measurement during 1.5 hr loading. In **c** and **d**, the signal intensity of the same two specimens (averaged over all caudal to cranial regions) is displayed against time (horizontal axis). The numbers in this row indicate the central (1) to peripheral (5) element rings.
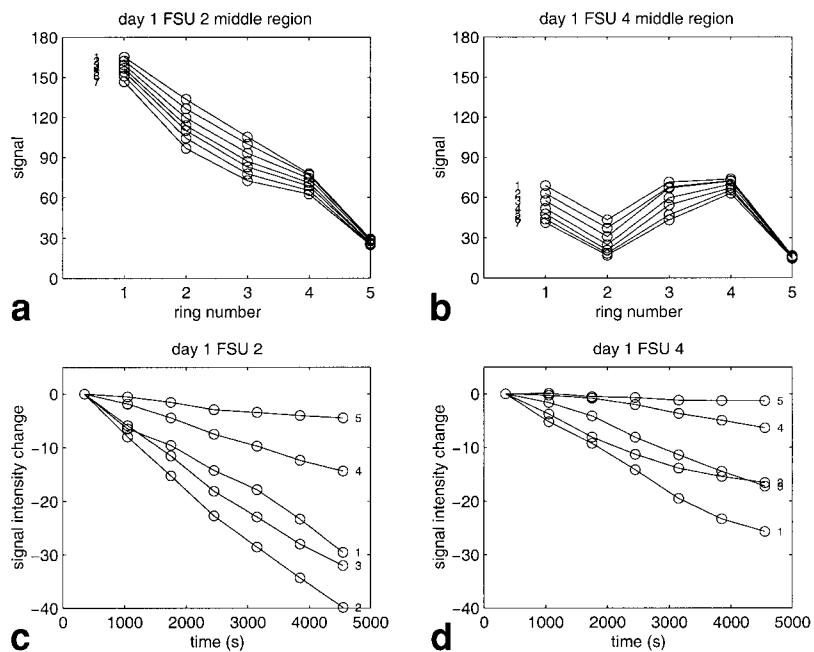
averaged over relatively large volumes. Separate tracking of small tissue particles would put higher demands on the accuracy of tissue properties in the model, including anisotropic tissue behavior.

The axial deformation curves, found in the current study, are comparable to curves found in human specimens (12,13). During axial deformation, the MRI measurements showed a gradual signal loss (being most pronounced in the central disc regions), presumably due to the loss of fluid. The status of human intervertebral discs is highly variable among subjects, especially dependent on age and degeneration status (14). Unexpectedly, we also found strong variations in the patterns of signal distribution between bovine specimens of comparable age. The general form of these patterns was reproduced on the second day, using independently constructed finite element models. For this reason, the variations over specimens can be attributed to actual structural variations and not to measurement or modeling errors.

The fact that specimens exhibited poor recovery from the first measurement, whereas intervertebral discs in vivo are known to recover overnight under comparable 250 N loading (9), is likely attributable to a reduced capacity of the tissue to take up water due to in vitro conditions (15)

and frozen storage (16). Therefore, the present results can not be generalized to in vivo loading.

In contrast to the present study, considerable signal loss during loading was found in the outermost element ring in a preliminary study with one porcine specimen (7). This difference may be attributable to a number of differences between the studies, i.e., a difference between species (bovine versus pig), vertebral region (coccygeal versus lumbar), pre-loading time (15 hr versus 30 min), prevention of dehydration (yes versus no), and inclusion of outermost tissue margin (no versus yes) for the current versus the previous study. In addition, TR was only 1200 msec in the previous study, so that $T_1$ influence can not be excluded in the earlier results.

Considering the long TR of 6000 msec, used in the present study, $T_1$ variations within the tissue can not have had a substantial influence on the MRI signal intensity. On the other hand, with a TE of 16 msec, $T_2$ changes with loading, which are known to occur in intervertebral disc tissue (17), can have a considerable influence on the MR signal. Consequently, the signal intensity may not be linearly related to the water content in the tissue. In order to estimate the magnitude of this effect, one additional FSU was dissected. The loading procedure was the same as in
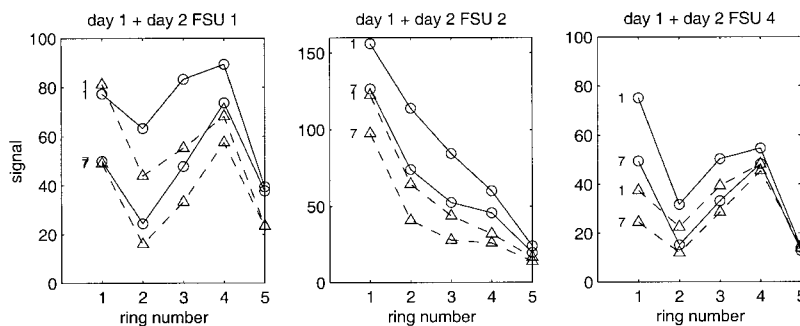


FIG. 5. Signal distribution over the central to peripheral element rings (horizontal axis) in three FSU's at the first (line 1) and last (line 7) MRI measurement during the 1.5 hr loading period. The solid and dashed lines indicate the first and second measurement day, respectively.
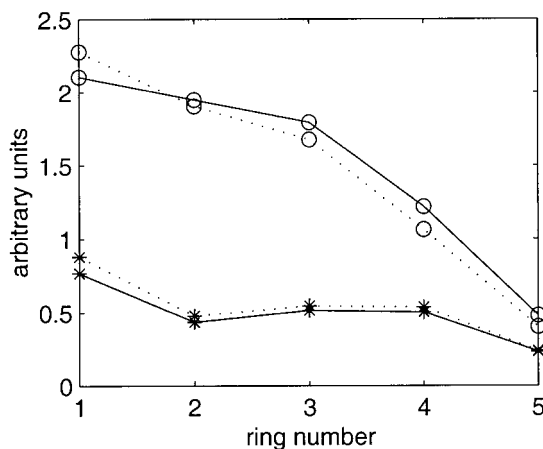
FIG. 6. Signal intensity in one additional specimen before (o) and after (*) 1.5 hr loading with 2000 N. The solid lines are based on normal signal intensities, the dashed lines are the same data, corrected for $T_2$ variations. Both the normal and corrected signal intensities are given in arbitrary units, where the average of the 10 relevant numbers (five for the five rings at the beginning and five for the five rings at the end of the loading period) was set to 1.

the other specimens, but now a series of MRI measurements was made with varying TE (16, 25, 35, and 50 msec, respectively), before and after the loading procedure. As before, a finite element model was constructed and deformed according to the measured axial displacement. Signal intensities were read into the finite element model and $T_2$ was estimated for each element. Before loading, a considerable variation of $T_2$ (ranging from 43 msec in the innermost disc region to 22 msec in the outermost region) was found within the disc. This is in line with findings of Chatani et al. (17), Weidenbaum et al. (18), and Antoniou et al. (14). After the loading period, the $T_2$ variation within the disc had largely disappeared. Following correction for $T_2$ variation, the overall patterns of signal distribution (at TE = 16 msec) before and after loading, were largely unchanged (Fig. 6).

In conclusion, the current study shows that a consistent pattern of gradual signal intensity changes is measured using finite element aided analysis of MR images of deforming intervertebral disc tissue. Between specimens, a remarkably large range in initial signal patterns was found, which probably is attributable to variations in tissue structure. The signal changes over time were rather consistent over specimens and suggested a strong fluid loss in the central portion of the intervertebral disc, less fluid loss in the intermediate region, and only marginal fluid loss in the outermost region of the disc. This is in accordance with data obtained from freeze-drying tissue samples of loaded and unloaded discs (5) and supports the notion that sus-

tained loading could, through the loss of fluid, affect the stress distribution within the intervertebral disc and the adjacent endplates.

Future studies will be directed towards a more time-efficient protocol, enabling the incorporation of $T_2$ quantification. In addition, incorporation of a set of images, optimized for contrast between disc, endplate, and bone, might improve the precision of the fit between model and tissue. Finally, the technique described in this study may also be applicable to other slowly deforming human tissues, both in vitro and in vivo.

## REFERENCES

1. Wedeen VJ. Magnetic resonance imaging of myocardial kinematics. Technique to detect, localize, and quantify the strain rates of the active human myocardium Magn Reson Med 1992;27:52–67.
2. McVeigh ER. MRI of myocardial function: motion tracking techniques Magn Reson Imag 1996;14:137–150.
3. Glover MG, Hargens AR, Mahmood MM, Gott S, Brown MD, Garfin SR. A new technique for the in vitro measurement of nucleus pulposus swelling pressure. J Orthop Res 1991;9:61–67.
4. Holm S, Nachemson A. Variations in the nutrition of the canine intervertebral disc induced by motion. Spine 1983;8:866–874.
5. McMillan DW, Garbutt G, Adams MA. Effect of sustained loading on the water content of intervertebral discs: implications for disc metabolism. Ann Rheum Dis 1996;55:1–8.
6. Zienkiewicz OC. The finite element method. Berkshire, UK: McGraw-Hill; 1983.
7. Kingma I, Weinans H, Dieën JH van, Boer RW de. Finite element aided tracking of signal intensity changes in deforming intervertebral disc tissue. Magn Reson Imag 1998;16:77–82.
8. Simon BR, Wu JSS, Carlton MW, Kazarian LE, France EP, Evans JH. Poroelastic dynamic structural models of rhesus spinal motion segments. Spine 1985;10:494–507.
9. Wilke HJ, Neef P, Caimi M, Hoogland T, Claes LE. New in vivo measurements of pressures in the intervertebral disc in daily life. Spine 1999;24:755–762.
10. Argoubi M, Shirazi-Adl A. Poroelastic creep response analysis of a lumbar motion segment in compression. J Biomechanics 1996;29:1331–1339.
11. Biot MA. General theory of three-dimensional consolidation. Journal of Applied Physics 1941;12:155–164.
12. Adams MA, Hutton WC. The effect of posture on the fluid content of lumbar intervertebral discs. Spine 1983;8:665–671.
13. Adams MA, McMillan DW, Green TP, Dolan P. Sustained loading generates stress concentrations in lumbar intervertebral discs. Spine 1996;21:434–8.
14. Antoniou J, Pike GB, Steffen T, Baramki H, Poole AR, Aebi M, Alini M. Quantitative magnetic resonance imaging in the assessment of degenerative disc disease. Magn Reson Med 1998;40:900–907.
15. Holmes AD, Hukins DW. Analysis of load-relaxation in compressed segments of lumbar spine. Med Eng & Phys 1996;18:99–104.
16. Bass EC, Duncan NA, Hariharan JS, Dusick J, Bueff HU, Lotz JC. Frozen storage affects the compressive creep behavior of the porcine intervertebral disc. Spine 1997;22:2867–2876.
17. Chatani K, Kusaka Y, Mifune T, Nishikawa H. Topographic differences of 1H-NMR relaxation times ($T_1$, $T_2$) in the normal intervertebral disc and its relationship to water content. Spine 1993;18:2271–2275.
18. Weidenbaum M, Foster RJ, Best BA, Saed-Nejad F, Nickoloff E, Newhouse J, Ratcliffe A, Mow VC. Correlating magnetic resonance imaging with the biochemical content of the normal human intervertebral disc. J Orthop Res 1992;10:552–61.